ISSN 1590-8844
International Journal of Mechanics and Control, Vol. XX, No. XX, 20XX

3-D ERLS based dynamic formulation for flexible-link robots: theoretical and numerical comparison between the Finite Element Method and the Component Mode Synthesis approaches

Renato Vidoni[*] Lorenzo Scalera[**] Alessandro Gasparetto[**]

[*] Free University of Bolzano, Bolzano, Italy

[**] University of Udine, Udine, Italy

ABSTRACT

The industrial demand for high-performance and low energy consume has highlighted the need to develop lightweight manipulators and robots. However, their design and control result more difficult with respect to rigid-link robotic systems mainly due to the structural flexibility of the arms. To this end, the Equivalent Rigid-Link System (ERLS) approach for 3-D flexible-link robots has been developed and, in this work, is considered in its recent developments. In particular, two recently published 3-D Equivalent Rigid-Link System formulations are discussed and compared by means of numerical simulations to highlight their strengths and possible weaknesses. The former deals with the Equivalent Rigid-Link System concept extension to spatial manipulators and robots through a Finite Element Method approach (ERLS-FEM), whereas the latter reformulates the model through a Component Mode Synthesis technique (ERLS-CMS). After the definition and discussion of the kinematic and dynamic equations, which account for the coupling between rigid-body and flexible-body motions, an extensive comparison is made. A benchmark manipulator is implemented and the formulations numerically compared in terms of accuracy and computational load under different input conditions.

Keywords: Equivalent Rigid-Link System; Component Mode Synthesis; Finite Element Method; flexible-link; dynamic model.

Nomenclature

$\boldsymbol{\alpha}$	angular acceleration terms vector
$\boldsymbol{\epsilon}$	strain vector
$\boldsymbol{\phi}$	angular virtual terms vector
$\boldsymbol{\theta}$	independent generalized coordinates vector
ρ	mass density
$\mathbf{a}$	linear acceleration terms vector
$\mathbf{C}$	compatibility matrix
$\mathbf{C}_d$	elastic terms compatibility matrix
$\mathbf{C}_r$	rigid terms compatibility matrix
$\mathbf{D}$	stress strain matrix
$\mathbf{e}$	node position vector
$\mathbf{f}$	concentrated external forces and torques vector
$\mathbf{f}_g$	equivalent nodal loads due to gravity vector
$\mathbf{G}$	matrix that contains the coefficients of the independent generalized coordinate acceleration
$\mathbf{g}$	gravity acceleration vector
$\mathbf{H}$	elastic energy matrix

Contact authors: Renato Vidoni[1], Lorenzo Scalera[2], Alessandro Gasparetto[2]. [1]Free University of Bolzano, Piazza Università, 5 39100 Bolzano (Italy). [2]University of Udine, via delle Scienze 206, 33100 Udine (Italy). E-mail: renato.vidoni@unibz.it, scalera.lorenzo@spes.uniud.it, alessandro.gasparetto@uniud.it

$\mathbf{J}$	Jacobian matrix
$\mathbf{K}$	stiffness matrix
$\mathbf{L}$	matrix that contains all terms not depending on virtual displacements and accelerations
$\mathbf{l}$	matrix that contains all terms not depending on virtual displacements
$\mathbf{M}$	mass matrix
$\mathbf{M}_C$	centrifugal stiffness terms matrix
$\mathbf{M}_G$	Coriolis terms matrix
$\mathbf{n}$	matrix that contains all terms not depending on both independent gereralized coordinate and modal coordinates accelerations
$\mathbf{P}$	linear virtual terms vector
$\mathbf{p}$	absolute nodal position vector
$\mathbf{q}$	modal coordinates vector
$\mathbf{q}_d$	elastic modal coordinates vector
$\mathbf{q}_r$	rigid modal coordinates vector
$\mathbf{S}$	joint displacements selector matrix
$\mathbf{T}$	local-to-local transformation matrix
$\mathbf{U}$	eigenvector
$\mathbf{u}$	node displacement vector
$\mathbf{V}_{\theta i}$	selection block-matrix for the rigid degrees of freedom
$\mathbf{V}_i^o$	selection matrix for the proper elements of the *i*th link
$\mathbf{V}_{qdi}$	selection block-matrix for the elastic modal coordinates
$\mathbf{V}_{qri}$	selection block-matrix for the rigid modal coordinates
$\mathbf{W}$	virtual work matrix
$\mathbf{W}_f$	generalized force work matrix
$\mathbf{W}_g$	gravitational force work matrix
$el.$	number of beam elements
I_c	shrink disk inertia
I_m	motor inertia
$m.$	number of modes
m_e	elbow articulation concentrated mass
AMM	Assumed Mode Method
CMS	Component Mode Synthesis
DoF	Degree of Freedom
ERLS	Equivalent Rigid-Link System
FEM	Finite Element Method

1 INTRODUCTION

Building a lightweight and high performance manipulator is one of the most important challenges in industrial robotics. Indeed, when lightening the system, dynamic effects of structural flexibility arise and both the design and control of the manipulator result more challenging and demanding. For an effective outcome it is crucial to have at our disposal accurate, manageable and possibly "computationally light" dynamic models.

In the last thirty years, researchers focused their attention on developing and refining dynamic formulations for describing the motion of multi-body rigid-flexible-link systems, from planar to spatial flexible-manipulators [23, 38, 28, 4, 40, 29, 12, 6, 31, 13, 20, 2, 27, 5]; however, thanks to the increasing computational capabilities of the industrial controllers and the availability of new high-strength and/or light materials, the research area is still an open field of investigation, especially with respect to 3-D systems and their control. Examples of recent modeling works of flexible manipulators and robots can be found in [3], [10] and [41].

By focusing on dynamical systems characterized by large displacements and small deformations, it is possible to develop a complete dynamic formulation where, given the rigid body dynamical model of the manipulator, the elastic deformations are introduced and a coupled approach that allows considering the mutual influence between rigid body motion and vibration can be obtained. However, the resultant formulation is highly non-linear with a coupled set of partial differential equations. Two main approaches to obtain a finite-dimensional problem have been proposed in literature: the "nodal" approach, i.e. the Finite Element Method (FEM), and the "modal" approach, i.e. the Assumed Mode Method (AMM) [29, 28, 12, 11, 17, 39, 24, 25, 26, 30, 22].

In the Finite Element Method a continuous domain can be represented as an amount of discrete sub-domains called elements. Each element is made of a fixed number of nodes, which define the number of degrees of freedom of the discrete system. In this way, it is possible to obtain mass and stiffness matrices which relate the forces applied in the nodes with nodal displacements and accelerations. A limitation of this methodology is that the number of degrees of freedom of the system should not be high if a low computational time (i.e. for real-time control purposes) is

required. On the other hand, the modal approach transforms the physical coordinates into a new reduced set of modal coordinates. Among all vibration modes only few of them are taken into account for the coordinates transformation: these comprehend all the modal coordinates related to the rigid motion of the system and at least one modal coordinate related to the main vibration mode. This approach is able to provide a reduced-order system of equations whose resolution is cheaper in terms of computational effort.

Among the different methods proposed in literature, in this work the Equivalent Rigid-Link System formulation, firstly introduced in [33, 32, 34, 8], is considered. Thanks to the Equivalent Rigid-Link System idea, two main advantages can be obtained: (a) the standard concepts of 3-D kinematics can be adopted to formulate and solve the system and (b) the kinematic equations of the Equivalent Rigid-Link System can be decoupled from the compatibility equations of the displacements at the joints.

The Equivalent Rigid-Link System concept has been applied, together with a Finite Element Method approach, to model planar flexible-link manipulators and robots by Giovagnoni in [18]. Then, the model has been linearised and exploited for control purposes [14, 15, 7]. In recent past, the formulation has been extended to treat 3-D systems [37, 36, 16] and, through a modal approach, to obtain a more flexible solution based upon a reduced-order system of equations [35]; in addition, the main differences and advantages with respect to the well known Floating Frame of Reference Formulation [29] have been described and discussed. The evolution of the ERLS-based dynamic model for flexible multibody systems has been presented in [5].

In this paper, after the description of the Equivalent Rigid-Link System kinematics for flexible-link robots (Section 2), the derivation of the virtual work term contributions and of the equations of motion for both the Equivalent Rigid-Link System - FEM and CMS methods is recalled (Section 3). Then, the main differences between the Finite Element Method and Component Mode Synthesis formulations are highlighted and discussed. Section 4 shows the numerical implementation and simulation of the models, whereas, in Section 5 the results of the numerical simulations are presented and discussed. Finally, Section 6 outlines the conclusions of this work.

2 EQUIVALENT RIGID-LINK SYSTEM KINEMATICS

By referring to Fig.1, being x, y, z a fixed global reference frame, $\mathbf{u}_i$ represents the nodal displacement vector of the *i*th link, $\mathbf{e}_i$ is the nodal position vector for the *i*th element of the ERLS and $\mathbf{p}_i$ is the absolute nodal position vector given by:

$$\mathbf{p}_i = \mathbf{e}_i + \mathbf{u}_i \tag{1}$$

The index i spans from 1 to l, where l is the number of links of the manipulator. Let x_i, y_i, z_i be a local reference frame, which follows the ERLS motion. It can be expressed with respect to the ERLS by means of a set of generalized coordinates $\boldsymbol{\theta}$, the m-rigid degrees of mobility of the mechanism, by exploiting the Denavit-Hartenberg notation that can be adopted to describe the kinematics of the ERLS. The $\mathbf{e}_i$'s can be gathered into a unique vector $\mathbf{e}$, representing the position and orientation of the whole ERLS, see Fig.1.

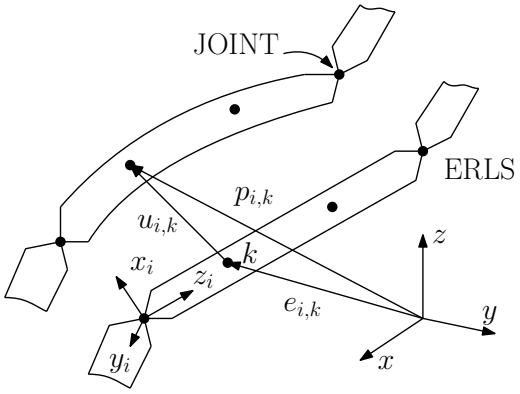

Figure 1 Model of the system and kinematic definitions.

To move from a nodal to a modal approach, the nodal displacements $\mathbf{u}_i$ of the *i*th link have to be firstly expressed as functions of a given number of eigenvectors $\mathbf{U}_i$ and modal coordinates $\mathbf{q}_i$, namely:

$$\mathbf{u}_i = \mathbf{U}_i \mathbf{q}_i \tag{2}$$

The eigenvectors and eigenvalues can be calculated according to the chosen modal (reduction) approach.

In terms of modal coordinates, the joint displacement belonging to link i and to link $i+1$ can be given by $\hat{\mathbf{u}_i} = \mathbf{S}_i \mathbf{U}_i \mathbf{q}_i$ and $\hat{\mathbf{u}_{i+1}} = \mathbf{S}_{i+1} \mathbf{U}_{i+1} \mathbf{q}_{i+1}$ respectively, where matrices $\mathbf{S}_i$ and $\mathbf{S}_{i+1}$ are introduced just to extract the proper joint displacement from all the nodal displacement. The compatibility condition at the *i*th joint is given by $\hat{\mathbf{u}_{i+1}} = \mathbf{T}_{i+1} \hat{\mathbf{u}_i}$, where $\mathbf{T}_{i+1}(\boldsymbol{\theta})$ is a local-to-local transformation matrix between two consecutive reference frames associated to the two consecutive links. By writing the previous equation for all the links and assembling them into a matrix, a comprehensive compatibility equation can be found:

$$\mathbf{C}(\boldsymbol{\theta})\mathbf{q} = 0 \tag{3}$$

Starting from this, the virtual displacements in the fixed reference frame and the acceleration of a generic point can be computed (see [35] for more details).

3 EQUIVALENT RIGID-LINK SYSTEM DYNAMICS

3.1 EQUIVALENT RIGID-LINK SYSTEM - FINITE ELEMENT METHOD DYNAMICS

The dynamic equations are obtained by applying the principle of virtual work and computing the inertial, elastic, gravity and external generalized forces terms:

$$\begin{aligned}&\delta\mathbf{W}^{inertia}+\delta\mathbf{W}^{elastic}=-\delta\mathbf{W}^{external}\\&\sum_i\int_{v_i}\delta\mathbf{p}_i^T\ddot{\mathbf{p}}_i\rho_i dv+\sum_i\int_{v_i}\delta\boldsymbol{\epsilon}_i^T\mathbf{D}_i\boldsymbol{\epsilon}_i dv=\\&\sum_i\int_{v_i}\delta\mathbf{p}_i^T\mathbf{g}\rho_i dv+(\delta\mathbf{u}^T+\delta\mathbf{e}^T)\,\mathbf{f}\end{aligned}\tag{4}$$

where ρ_i, $\mathbf{D}_i$ and $\boldsymbol{\epsilon}_i$ are the mass density, the stress-strain matrix and the strain vector for the *i*th volume (finite) element, $\mathbf{g}$ is the gravity acceleration vector, and $\mathbf{f}$ is the vector of the concentrated external forces and torques; $\delta\mathbf{u}$ and $\delta\mathbf{e}$ refer to all the nodes of the model. The nodal elastic virtual displacements $\delta\mathbf{u}$ and the virtual displacements of the Equivalent Rigid-Link System $\delta\mathbf{e}$ are completely independent. Thus, two set of equilibrium equations, i.e. local nodal equilibrium and global equilibrium equations, can be obtained from Eq.4 by zeroing alternatively the nodal elastic virtual displacements and the virtual displacements of the ERLS. The following system of differential equations are obtained:

$$\begin{aligned}&\mathbf{M}(\ddot{\mathbf{e}}+\ddot{\mathbf{u}})+2(\mathbf{M}_{G1}+\mathbf{M}_{G2})\dot{\mathbf{u}}+\\&(\mathbf{M}_{C1}+2\mathbf{M}_{C2}+\mathbf{M}_{C3})\mathbf{u}+\mathbf{K}\mathbf{u}=\\&\mathbf{f}_g+\mathbf{f}\end{aligned}\tag{5}$$

$$\begin{aligned}&\mathbf{J}^T\mathbf{M}(\ddot{\mathbf{e}}+\ddot{\mathbf{u}})+2\mathbf{J}^T(\mathbf{M}_{G1}+\mathbf{M}_{G2})\dot{\mathbf{u}}+\\&\mathbf{J}^T(\mathbf{M}_{C1}+2\mathbf{M}_{C2}+\mathbf{M}_{C3})\mathbf{u}=\\&\mathbf{J}^T(\mathbf{f}_g+\mathbf{f})\end{aligned}\tag{6}$$

where $\mathbf{M}$ is the mass matrix, $\mathbf{M}_{G1}$ and $\mathbf{M}_{G2}$ are the Coriolis terms, $\mathbf{M}_{C1}$, $\mathbf{M}_{C2}$ and $\mathbf{M}_{C3}$ the centrifugal stiffness terms, $\mathbf{K}$ the stiffness matrix, $\mathbf{J}$ the Jacobian matrix, that allows to express the $\delta\mathbf{e}$ virtual displacements with respect to the $\delta\boldsymbol{\theta}$ independent generalized coordinates, and $\mathbf{f}_g$ the vector of the equivalent nodal loads due to gravity. The dynamic equations, after the substitution of the second order differential kinematics equations of the ERLS, can be grouped and rearranged in matrix form, as it can be seen in Eq.7, where $\mathbf{M}_{G12}=\mathbf{M}_{G1}+\mathbf{M}_{G2}$ and $\mathbf{M}_{C123}=\mathbf{M}_{C1}+2\mathbf{M}_{C2}+\mathbf{M}_{C3}$. See [37] and [36] for further details.

$$\begin{aligned}&\left[\begin{array}{c|c}\mathbf{M}&\mathbf{M}\mathbf{J}\\\mathbf{J}^T\mathbf{M}&\mathbf{J}^T\mathbf{M}\mathbf{J}\end{array}\right]\left[\begin{array}{c}\ddot{\mathbf{u}}\\\ddot{\boldsymbol{\theta}}\end{array}\right]=\\&\left[\begin{array}{c|c|c}-2\mathbf{M}_{G12}&-\mathbf{M}\dot{\mathbf{J}}&-\mathbf{M}_{C123}-\mathbf{K}\\-\mathbf{J}^T2\mathbf{M}_{G12}&-\mathbf{J}^T\mathbf{M}\mathbf{J}&-\mathbf{J}^T\mathbf{M}_{C123}\end{array}\right]\left[\begin{array}{c}\dot{\mathbf{u}}\\\dot{\boldsymbol{\theta}}\\\boldsymbol{\theta}\end{array}\right]+\\&\left[\begin{array}{c|c}\mathbf{M}&\mathbf{I}\\\mathbf{J}^T\mathbf{M}&\mathbf{J}^T\end{array}\right]\left[\begin{array}{c}\mathbf{f}_g\\\mathbf{f}\end{array}\right]\end{aligned}\tag{7}$$

A Rayleigh model of damping can be eventually considered and inserted in the model to deal with real flexible manipulator systems.

3.2 EQUIVALENT RIGID-LINK SYSTEM - COMPONENT MODE SYNTHESIS DYNAMICS

In a similar manner, starting from the formulation of the velocity/virtual displacement and acceleration terms as functions of $\boldsymbol{\theta}$, i.e. the independent generalized coordinates, and $\mathbf{q}_d$, i.e. the independent modal coordinates, and their derivatives, the virtual work contributions can be derived. Then, the relationship between the velocities/virtual displacements and accelerations of the rigid body modal coordinates $\mathbf{q}_r$ and the velocities/virtual displacements and accelerations of the independent variables, see [35] for the details, can be recalled:

$$\delta\mathbf{q}_r=\mathbf{D}(\boldsymbol{\theta})\delta\mathbf{q}_d+\mathbf{G}(\boldsymbol{\theta},\mathbf{q})\delta\boldsymbol{\theta}\tag{8}$$

$$\ddot{\mathbf{q}}_r=\mathbf{G}(\boldsymbol{\theta},\mathbf{q})\ddot{\boldsymbol{\theta}}+\mathbf{D}(\boldsymbol{\theta})\ddot{\mathbf{q}}_d+\mathbf{n}(\boldsymbol{\theta},\dot{\boldsymbol{\theta}},\mathbf{q},\dot{\boldsymbol{q}})\tag{9}$$

where the matrices $\mathbf{D}(\boldsymbol{\theta})$, $\mathbf{G}(\boldsymbol{\theta},\mathbf{q})$ and the vector $\mathbf{n}(\boldsymbol{\theta},\dot{\boldsymbol{\theta}},\mathbf{q},\dot{\boldsymbol{q}})$ take into account the different contributions and dependencies. In particular, $\mathbf{D}(\boldsymbol{\theta})$ is the matrix which relates the rigid modal coordinates $\mathbf{q}_r$ and the elastic modal ones $\mathbf{q}_d$:

$$\mathbf{q}_r=\mathbf{D}(\boldsymbol{\theta})\mathbf{q}_d\tag{10}$$

and it is defined as:

$$\mathbf{D}(\boldsymbol{\theta})=-\mathbf{C}_r^+(\boldsymbol{\theta})\mathbf{C}_d(\boldsymbol{\theta})\tag{11}$$

where $\mathbf{C}_r$ and $\mathbf{C}_d$ contain the coefficients of the rigid and elastic modal coordinates and only depend on the joint parameters. These matrices are obtained by rearranging the comprehensive compatibility equation (Eq.3) into the rigid and the modal contributions as follows:

$$\mathbf{C}_r\mathbf{q}_r+\mathbf{C}_d\mathbf{q}_d=0\tag{12}$$

Starting from Eq.8, the virtual terms of the generic *i*th link, i.e. linear $\delta\mathbf{P}_{0i}$, angular $\delta\boldsymbol{\phi}_i$ and modal $\delta\mathbf{q}$, can be written as:

$$\begin{aligned}&\begin{bmatrix}\delta\mathbf{P}_{0i}\\\delta\boldsymbol{\phi}_i\\\delta\mathbf{q}\end{bmatrix}=\\&\begin{bmatrix}\boldsymbol{V}_{\theta i}&\mathbf{0}&\mathbf{0}\\\mathbf{0}&\boldsymbol{V}_{qri}&\mathbf{0}\\\mathbf{0}&\mathbf{0}&\boldsymbol{V}_{qdi}\end{bmatrix}\begin{bmatrix}\mathbf{J}(\boldsymbol{\theta})&\mathbf{0}\\\mathbf{G}(\boldsymbol{\theta},\mathbf{q})&\mathbf{D}(\boldsymbol{\theta})\\\mathbf{0}&\mathbf{I}\end{bmatrix}\begin{bmatrix}\delta\boldsymbol{\theta}\\\delta\mathbf{q}_d\end{bmatrix}=\\&\mathbf{V}_i^o\mathbf{N}\begin{bmatrix}\delta\boldsymbol{\theta}\\\delta\mathbf{q}_d\end{bmatrix}\end{aligned}\tag{13}$$

where $\mathbf{V}_i^o$ is a selection matrix for the proper elements of the *i*th link ($\boldsymbol{V}_{\theta i}$ is the selection block-matrix for the rigid DoFs,

$\boldsymbol{V}_{qri}$ for the rigid modal coordinates and $\boldsymbol{V}_{qdi}$ for the elastic modal ones) and $\mathbf{J}(\boldsymbol{\theta})$ the Jacobian matrix of the Equivalent Rigid-Link System. The $\mathbf{V}_i^o$ matrix is block diagonal and allows to select the correct terms related to both the rigid degrees of freedom and the independent vibration modal coordinates. Also the acceleration terms (Eq.9), i.e. linear $\mathbf{a}_{0i}$, angular $\boldsymbol{\alpha}_i$ and modal $\ddot{\boldsymbol{q}}$, can be rewritten as function of the independent variables:

$$\begin{bmatrix} \mathbf{a}_{0i} \\ \boldsymbol{\alpha}_i \\ \ddot{\boldsymbol{q}} \end{bmatrix} = \mathbf{V}_i^o \mathbf{N} \begin{bmatrix} \ddot{\boldsymbol{\theta}} \\ \ddot{\boldsymbol{q}}_{\boldsymbol{d}} \end{bmatrix} + \mathbf{V}_i^o \begin{bmatrix} \dot{\boldsymbol{J}}(\boldsymbol{\theta}, \dot{\boldsymbol{\theta}}) \dot{\boldsymbol{\theta}} \\ \boldsymbol{n}(\boldsymbol{\theta}, \dot{\boldsymbol{\theta}}, \boldsymbol{q}, \dot{\boldsymbol{q}}) \\ \mathbf{0} \end{bmatrix} \tag{14}$$

The second term of the equation depends only on the position and velocity of the independent variables and, thus, it is known.
The virtual work done by the inertial forces can be split into two contributes:

$$\delta \mathbf{W}_{inertia} = \delta \mathbf{W}^I_{inertia} + \delta \mathbf{W}^{II}_{inertia} \tag{15}$$

where the former contains all of the terms related to the second derivative of the variables, the latter contains all the remaining terms. The virtual work done by the inertial forces $\delta \mathbf{W}^I_{inertia,i}$ and $\delta \mathbf{W}^{II}_{inertia,i}$ of each link, and the virtual works done by the gravitational $\delta \mathbf{W}_g$ and generalized $\delta \mathbf{W}_f$ forces, can be written as:

$$-\delta \mathbf{W}^I_{inertia,i} = \begin{bmatrix} \delta \mathbf{P}_{0i}^T & \delta \boldsymbol{\phi}_i^T & \delta \mathbf{q}^T \end{bmatrix} \mathbf{L}_i \begin{bmatrix} \mathbf{a}_{0i} \\ \boldsymbol{\alpha}_i \\ \ddot{\boldsymbol{q}} \end{bmatrix} \tag{16}$$

where the $\mathbf{L}_i$ matrix contains all the terms not depending on virtual displacements and accelerations.
By substituting Eq.13 and Eq.14, it holds:

$$-\delta \mathbf{W}^I_{inertia,i} = \begin{bmatrix} \delta \boldsymbol{\theta}^T & \delta \mathbf{q}_d^T \end{bmatrix} \mathbf{N}^T \mathbf{V}_i^{oT} \mathbf{L}_i \left(\mathbf{V}_i^o \mathbf{N} \begin{bmatrix} \ddot{\boldsymbol{\theta}} \\ \ddot{\boldsymbol{q}}_{\boldsymbol{d}} \end{bmatrix} + \mathbf{V}_i^o \begin{bmatrix} \dot{\boldsymbol{J}}(\boldsymbol{\theta}, \dot{\boldsymbol{\theta}}) \dot{\boldsymbol{\theta}} \\ \mathbf{n}(\boldsymbol{\theta}, \dot{\boldsymbol{\theta}}, \mathbf{q}, \dot{\boldsymbol{q}}) \\ \mathbf{0} \end{bmatrix} \right) \tag{17}$$

$$\delta \mathbf{W}^{II}_{inertia,i} = \begin{bmatrix} \delta \mathbf{P}_{0i}^T & \delta \boldsymbol{\phi}_i^T & \delta \mathbf{q}^T \end{bmatrix} \mathbf{l}_i = \begin{bmatrix} \delta \boldsymbol{\theta}^T & \delta \mathbf{q}_d^T \end{bmatrix} \mathbf{N}^T \mathbf{V}_i^{oT} \mathbf{l}_i \tag{18}$$

All the other terms such as the variation of the elastic energy $\delta \mathbf{H}$, the gravitational forces $\delta \mathbf{W}_g$ and the resultant generalized forces $\delta \mathbf{W}_f$ do not depend on accelerations. Then, they can be gathered into a unique term $\tilde{\boldsymbol{l}}_{\boldsymbol{i}}$. By naming $\delta \mathbf{W}_i$ the term with all the contributions not depending on accelerations, it holds:

$$\delta \mathbf{W}_i = \begin{bmatrix} \delta \mathbf{P}_{0i}^T & \delta \boldsymbol{\phi}_i^T & \delta \mathbf{q}^T \end{bmatrix} \tilde{\boldsymbol{l}}_{\boldsymbol{i}} = \begin{bmatrix} \delta \boldsymbol{\theta}^T & \delta \mathbf{q}_d^T \end{bmatrix} \mathbf{N}^T \mathbf{V}_i^{oT} \tilde{\boldsymbol{l}}_{\boldsymbol{i}} \tag{19}$$

All the links contributions can be added to obtain the final formulation:

$$-\delta \mathbf{W}^I_{inertia} = \sum_{i=1}^{N} \begin{bmatrix} \delta \boldsymbol{\theta}^T & \delta \mathbf{q}_d^T \end{bmatrix} \mathbf{N}^T \mathbf{V}_i^{oT} \mathbf{L}_i \left(\mathbf{V}_i^o \mathbf{N} \begin{bmatrix} \ddot{\boldsymbol{\theta}} \\ \ddot{\boldsymbol{q}}_{\boldsymbol{d}} \end{bmatrix} + \mathbf{V}_i^o \begin{bmatrix} \dot{\boldsymbol{J}}(\boldsymbol{\theta}, \dot{\boldsymbol{\theta}}) \dot{\boldsymbol{\theta}} \\ \mathbf{n}(\boldsymbol{\theta}, \dot{\boldsymbol{\theta}}, \mathbf{q}, \dot{\boldsymbol{q}}) \\ \mathbf{0} \end{bmatrix} \right) =$$

$$= \delta \mathbf{W} = \sum_{i=1}^{N} \begin{bmatrix} \delta \boldsymbol{\theta}^T & \delta \mathbf{q}_d^T \end{bmatrix} \mathbf{N}^T \mathbf{V}_i^{oT} \tilde{\boldsymbol{l}}_{\boldsymbol{i}}$$

By naming $\mathbf{L} \stackrel{\text{def}}{=} \sum_{i=1}^{N} \mathbf{V}_i^{oT} \mathbf{L}_i \mathbf{V}_i^o$ and $\tilde{\boldsymbol{l}} \stackrel{\text{def}}{=} \sum_{i=1}^{N} \mathbf{V}_i^{oT} \tilde{\boldsymbol{l}}_{\boldsymbol{i}}$, and discarding the virtual displacements, the final dynamic model results:

$$\mathbf{N}^T \mathbf{L} \mathbf{N} \begin{bmatrix} \ddot{\boldsymbol{\theta}} \\ \ddot{\boldsymbol{q}}_{\boldsymbol{d}} \end{bmatrix} = \mathbf{N}^T \left(\mathbf{L} \left(- \begin{bmatrix} \dot{\boldsymbol{J}}(\boldsymbol{\theta}, \dot{\boldsymbol{\theta}}) \boldsymbol{\theta} \\ \mathbf{n}(\boldsymbol{\theta}, \dot{\boldsymbol{\theta}}, \mathbf{q}, \dot{\boldsymbol{q}}) \\ \mathbf{0} \end{bmatrix} \right) + \tilde{\mathbf{l}} \right) \tag{20}$$

3.3 THEORETICAL COMPARISON

With respect to the Equivalent Rigid-Link System - Finite Element Method formulation, the Component Mode Synthesis model:

- takes into account all the terms without simplifications and/or neglecting some, even if with a small contribution, inertia coupling terms. Indeed, in the virtual displacement formulation of the ERLS-FEM approach, the terms with lower-order magnitude are usually neglected [37];
- allows to work with whatsoever flexible or rigid-link shape and finite elements thanks to the modal representation; the Equivalent Rigid-Link System - Finite Element Method usually deals with flexible beam type links;
- allows, as already explained, to reduce the complexity of the model and possibly maintain a number of degrees of freedom that can be handled by a processor when a fine discretization is needed;
- allows the choice of a specific number of equations, which globally describes the dynamic behaviour of the flexible system;
- allows to retain only the interior modes of interest (e.g. by using the Craig-Bampton approach [9]).

4 NUMERICAL IMPLEMENTATION AND SIMULATION

The Finite Element Method and Component Mode Synthesis dynamic models have been implemented in Matlab™ environment and test them. Different benchmark mechanisms have been proposed in literature, such as single-link, planar, closed loop and spatial manipulators (e.g. [12, 18, 7, 21, 19, 1]). In this work, looking at a 3-D motion and excitation,

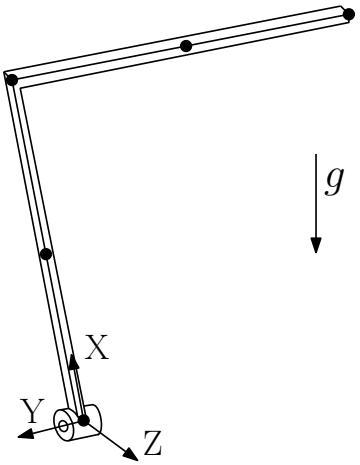

Figure 2 L-shaped manipulator: reference frame and possible node discretization.

a L-shaped mechanism, already adopted in [35], has been chosen.
The L-shape, basically made of two flexible rods (Fig.2), allows to induce motion and vibrations in different directions. For the ERLS-CMS model, the link flexibility has been imported through a special file, i.e. the modal neutral file, generated in Ansys™ and based on the Craig-Bampton reduction.
The L-shaped system has one rigid rotational DoF and, in these tests, it has been modeled with two and four Euler-Bernoulli beams - Finite Elements - in Ansys™. Even if a low number of FE is considered, a good representation of its dynamic behaviour can be obtained [35, 14, 7, 16]. Each Euler-Bernoulli beam has two nodes and six degrees of freedom: the two-elements system has a total of 18 DoFs whereas the four-elements one has a total of 30 DoFs.
The geometrical and mechanical parameters of the chosen mechanism are reported in Tab.I.
To compare the different formulations, the mechanism responses under different inputs have been evaluated. In particular, as made also in other works [35, 18, 21, 19], gravitational force and torque inputs (see Fig.s 2 and 3) have been considered and the results compared. Gravitational force has been chosen as a natural way to excite the system, whereas the step torque input allows to properly excite the 3-D mechanism upon a wider range of frequencies.
The input signal allows, from a statically balanced configuration at $135°$, to fast accelerate and decelerate. For simulating a realistic mechanical system, a motor inertia I_m, a shrink disc inertia I_c and an elbow articulation concentrated mass m_e have been added to the model. The chosen values are $I_m = 0.0043\ kg\ m^2$, $I_c = 0.001269\ kg\ m^2$ and $m_e = 0.017\ kg$, respectively.

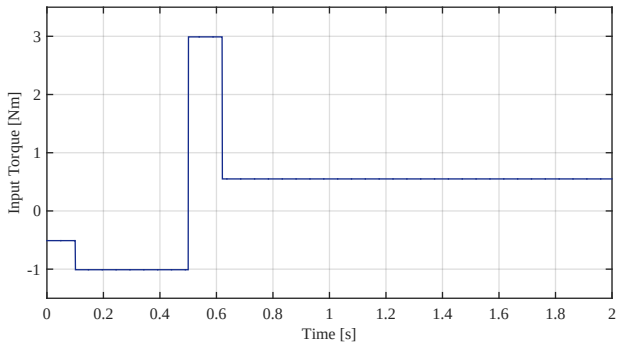

Figure 3 Input torque signal.

The number of exported modes is defined in Ansys™ when creating the *.mnf* file for Adams™ that exploits a Craig-Bampton approach. In the 2-elements case, all available modes have been exported whereas in the 4-elements case both 18 and 30, over the 30 available modes, have been chosen. In Tab.II, the exported natural frequencies have been reported. The first 6 values are not present since they are equal to zero representing rigid-body modes.
In Tab.III the properties of the laptop used for numerical simulations are reported.
For each subdivision of the L-shaped manipulator in beam elements, different numerical simulations have been run, by varying the number of considered modes. The dynamics of the robotic system has been simulated for a time equal to 2 seconds and by adopting a variable step *ode45* solver, based on an explicit Runge-Kutta formulation. For each number of considered modes, three simulations have been run in order to obtain a correct average value of computational time.

5 RESULTS AND DISCUSSION

In this section, the results of the numerical simulations for the L-shaped manipulator subjected to both gravity and torque inputs are presented. Dynamic simulations of the mechanism under gravity are intended to show the L-shaped system frequency response over a large frequency domain, whereas simulations under torque input highlight the behaviour of the system under a forced condition, more similar to a real application.
In particular, four significant cases are highlighted and focused:

- the 2- and 4-elements models without reduction equivalent to the ERLS-FEM 2- and 4-beam elements model, i.e. 2 el. 18/18 modes and 4 el. 30/30 modes;
- the 4-elements model exported from Ansys™ with 18 modes, i.e. 4 el. 18/18 modes;
- the model obtained by the full 30/30 reduced choosing only the first 18 modes, i.e. 4 el. 18/30 modes.

Table I - Geometrical and mechanical parameters of the L-shaped manipulator.

Rod	Material	Length [m]	Depth [m]	Width [m]	Density [kg/m^3]	Poisson's ratio	Young's module [N/m^2]
1^{st}	Aluminium	0.5	0.008	0.008	2700	0.33	7e^{10}
2^{nd}	Aluminium	0.5	0.008	0.008	2700	0.33	7e^{10}

Table II - Natural frequencies [Hz] obtained by Adams^{TM} report files.

Mode	2 el. (18 m.)	4 el. (18 m.)	4 el. (30 m.)	Mode	4 el. (30 m.)
7	23.33	28.19	28.19	19	5466.76
8	37.56	34.42	34.42	20	6104.64
9	1171.02	103.24	103.25	21	6104.64
10	1273.62	106.16	106.16	22	6483.02
11	2519.98	187.01	186.90	23	7991.92
12	2729.22	234.08	234.08	24	11313.76
13	2729.22	1434.45	1344.65	25	14071.89
14	3241.51	1463.87	1371.12	26	18313.23
15	5427.78	3761.82	3360.82	27	19697.79
16	9207.15	6368.74	3379.20	28	23294.27
17	10398.16	7310.70	3507.58	29	23651.84
18	12610.60	12023.24	3508.01	30	25068.96

Table III - Hardware used for the numerical simulations.

Computer	HP Pavillon dv6
Processor	Intel® Core^{TM} 2 Duo CPU T6400 @ 2.00 GHz 2.00 GHz
Installed memory (RAM)	4.00 GB
System type	64-bit Operating System, x64-based processor
Windows edition	Windows 10 Pro

5.1 MECHANISM UNDER GRAVITY

To better appreciate the differences between Finite Element Method and Component Mode Synthesis model results, the tip z-coordinate acceleration signal of the L-shaped manipulator under gravity both in the time and frequency domains are reported in Fig.s 4(a) and 4(b). The z-coordinate has been chosen since it is the one that is heavily excited due to the considered external forces acting on the mechanism and, therefore, allows a better comparison of the results.

The 4-elements 18-modes and the 4-elements 30-modes signals overlap almost perfectly whereas, as it can be expected, the 2-elements signal shows a good agreement only at low frequencies. Small differences can be observed for the 4 el. 18/30 modes case due to the post reduction in the mode number.

In Tab.IV, the resonance peaks, detected on the z-coordinate acceleration signal of the L-shaped mechanism, are reported. Only frequencies lower than $10\ kHz$ have been considered here. Looking at the values, it can be highlighted how, in both the 4-elements cases, i.e. 4 el. 18 exported modes and 4 el. 30 modes, 14 vibration modes can be sufficient to obtain a very good agreement of the first 8 resonance peaks with respect to the Finite Element Method case, i.e. full model condition.

Concerning simulation results with a considered number of modes lower than 14, a good agreement can be found only with respect to the first 3 peaks.

As expected, by increasing the number of considered modal coordinates the resonance peaks shift to lower frequency values.

In Tab.V and Fig.5 the computational time for each simulation is given, whereas in Tab.VI the mean computational time over the three simulations of each case and the percentage reduction with respect to the computational time of the FEM cases, i.e. the cases with no modal reduction, are shown.

It can be noticed that, for the 2-elements 18-modes and 4-elements 30-modes, the percentage reduction of computational effort is always greater than 50 $\%$. An important computational time reduction can be appreciated also for the 4-elements 18-modes with respect to both 2 and 4-elements FEM.

By considering the four main cases previously evaluated, it can be appreciated how the modal reduction at 18 modes, i.e. 18 imported modes, allows a time saving of about 22 $\%$ whereas, if 18 modes are maintained from the 4el 30 modes case, the time saving increases up to about 72 $\%$.

If the 14 modes condition is evaluated, i.e. the one that allows to have an agreement on the first 8 resonance peaks, it can be appreciated how the reduction in time is always greater than 88 $\%$, thus allowing to highlight the better performances of the ERLS-CMS approach with respect to the ERLS-FEM one.

Table IV - Resonance peaks [Hz] with respect to beam elements and considered modes, mechanism subjected to gravity force.

Elements	Modes	Resonance peaks [Hz]										
		1	2	3	4	5	6	7	8	9	10	11
2 (18 m.)	18	0.5	7.5	28	31.5	1482						
4 (18 m.)	8	0.5	12	28.5								
	10	0.5	10	26.5	38							
	12	0.5	8.5	26	37.5	124.5	170					
	14	0.5	9	11.5	25.5	30.5	111.5	124	172	1464		
	16	0.5	9	11.5	25.5	30.5	111.5	124	172	2259	6163	
	18	0.5	8.5	11.5	24	30.5	111.5	117	172	265.5	2260	9334
4 (30 m.)	8	0.5	12	28.5								
	10	0.5	10	26.5	38							
	12	0.5	9.5	26	37.5	124	170					
	14	0.5	9	12	25.5	30.5	112.5	124	172	1371		
	16	0.5	9	11.5	25.5	30.5	111.5	124	172	3381		
	18	0.5	9	11.5	25.5	30.5	111.5	124	172	1918	3429	
	30	0.5	8.5	11.5	24	30.5	111.5	117	172	265.5	1767	5044

Table V - Computational time [s], mechanism under gravity.

Elements	Modes							
	6	8	10	12	14	16	18	30
2 (18 m.)	1.31	6.53	226.34	437.91	466.41	1041.23	2160.01	
	0.99	5.69	196.42	371.03	442.32	1004.10	2120.68	
	1.61	6.29	220.39	387.06	467.94	1027.24	2114.84	
4 (18 m.)	1.24	6.02	6.38	27.69	245.81	1128.18	1667.27	
	0.99	5.86	6.39	26.40	234.17	1046.00	1608.18	
	1.12	5.88	6.53	26.69	236.03	1085.86	1636.31	
4 (30 m.)	1.21	6.11	6.47	27.62	218.68	583.11	589.64	4969.19
	1.47	5.80	6.47	27.07	221.09	614.76	622.72	5024.79
	1.45	5.69	6.44	28.47	232.38	623.67	581.73	4974.43

Table VI - Computational mean time [s] and reduction [%] with respect to the FEM case, mechanism under gravity.

Elements		Modes					
		10	12	14	16	18	30
2 (18 m.)	mean time [s]	214.38	398.67	458.89	1024.19	2098.84*	
	* [%]	89.79	81.01	78.14	51.20		
4 (30 m.)	mean time [s]	6.46	27.72	224.05	607.18	598.03	4989.47**
	* [%]	99.69	98.68	89.33	71.07	71.94	
	** [%]	99.87	99.44	95.51	87.83	88.01	
4 (18 m.)	mean time [s]	6.43	26.93	238.67	1086.68	1637.25	
	* [%]	99.69	98.72	88.63	48.22	21.99	
	** [%]	99.87	99.46	95.22	78.22	67.19	
Reduction with respect to		*					
Reduction with respect to		**					

5.2 MECHANISM SUBJECTED TO TORQUE INPUT

The tip z-coordinate acceleration of the L-shaped beam under torque input is reported in Fig.6(a) and 6(b) in time and frequency domain.

In these cases, as well as in the gravitational force ones, the 4-elements acceleration signals match each other very well, whereas the 2- elements FEM captures only the low frequencies in a good manner.

Tab.VII shows the resonance peaks of the previous acceleration signals; it can be found that, for both 4-elements cases, only 14 modal coordinates in input are enough to identify the first 4 resonance peaks. The general trend is quite similar to the gravitational force case, since resonance peaks shift on lower frequency values whereas increasing the number of considered modes. With respect to the gravity case, the torque case shows 6 main excited frequencies.

Table VII - Resonance peaks [Hz] with respect to beam elements and considered modes, mechanism subjected to torque input.

Elements	Modes	Resonance peaks [Hz]					
		1	2	3	4	5	6
2 (18 m.)	18	9.5	32.5	1491	11720		
4 (18 m.)	8	28.5					
	10	26.5	38				
	12	26.5	37.5	170			
	14	11.5	30.5	111.5	172		
	16	11	30.5	111.5	172	2271	6163
	18	11	30.5	111.5	172	2272	9345
4 (30 m.)	8	28.5					
	10	26.5	38				
	12	26.5	37.5	170			
	14	12	30.5	113	172		
	16	11	30.5	111.5	172		
	18	11	30.5	111.5	172	1929	3440
	30	11	30.5	111.5	172	1755	1778

Table VIII - Computational time [s], mechanism subjected to torque input.

Elements	Modes							
	6	8	10	12	14	16	18	30
2 (18 m.)	1.02	5.85	203.64	387.05	454.47	1002.56	2091.69	
	1.37	6.35	213.72	374.69	445.70	1021.75	2105.60	
	1.42	5.62	198.73	378.21	448.13	986.64	2055.80	
4 (18 m.)	1.09	5.38	5.85	30.23	255.47	1070.51	1678.88	
	1.06	5.15	5.81	29.13	244.35	1053.85	1625.22	
	1.19	5.32	6.13	31.08	259.08	1087.85	1721.40	
4 (30 m.)	1.23	5.41	6.18	29.31	219.46	578.43	591.33	5137.08
	1.33	5.31	6.16	30.27	219.47	573.86	591.82	5127.65
	1.41	5.56	6.51	30.44	229.45	590.09	635.96	5087.46

Table IX - Computational mean time [s] and reduction [%] with respect to the FEM case, mechanism subjected to torque input.

Elements		Modes					
		10	12	14	16	18	30
2 (18 m.)	mean time [s]	205.36	379.98	449.43	1003.65	2084.36*	
	* [%]	90.15	81.77	78.44	51.85		
4 (30 m.)	mean time [s]	6.28	30.01	222.79	580.79	606.37	5117.40**
	* [%]	99.70	98.56	89.31	72.14	70.91	
	** [%]	99.88	99.41	95.65	88.65	88.15	
4 (18 m.)	mean time [s]	5.93	30.15	252.97	1070.74	1675.17	
	* [%]	99.72	98.55	87.86	48.63	19.63	
	** [%]	99.88	99.41	95.06	79.08	67.27	
Reduction with respect to		*					
Reduction with respect to		**					

In Tab.VIII and in Fig.7 the computational time of the different simulations is reported. As it can be seen, the computational time decreases by increasing the number of beam elements and the exported modes, for each number of considered modes. By increasing the beam elements and choosing the same number of modes, lower natural frequencies are considered, see Tab.II. Thus, the solver is able to extend the time integration step and therefore the required computational time decreases.

By considering the four main cases previously evaluated, it can be appreciated how the modal reduction at 18 modes, i.e. 18 imported modes, allows a time saving of about 20 $\%$ whereas, if 18 modes are maintained from the 4 el. 30 modes case, the time saving increases up to about 71 $\%$.

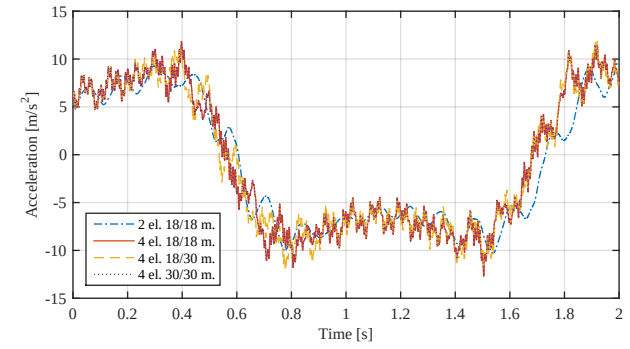

(a) Time domain.

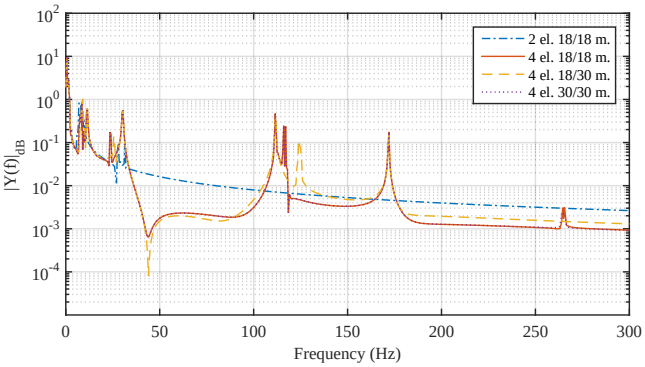

(b) Frequency domain.

Figure 4 Comparison of the tip z-coordinate acceleration of the L-shaped mechanism under gravity force. At the beginning of the excitation, the manipulator is in a static balanced position at 135°.

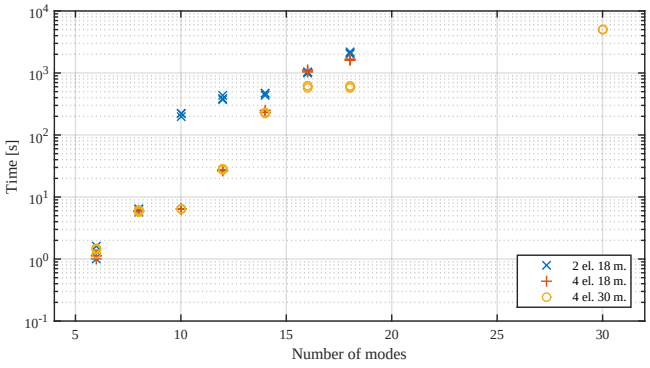

Figure 5 Computational time [s] in logarithmic scale, mechanism under gravity.

If the 14 modes condition is evaluated, i.e. the one that allows to have an agreement on the first 4 resonance peaks, it can be appreciated how the time reduction is again always greater than 88 %, thus allowing to highlight the better performances of the ERLS-CMS approach with respect to the ERLS-FEM one.

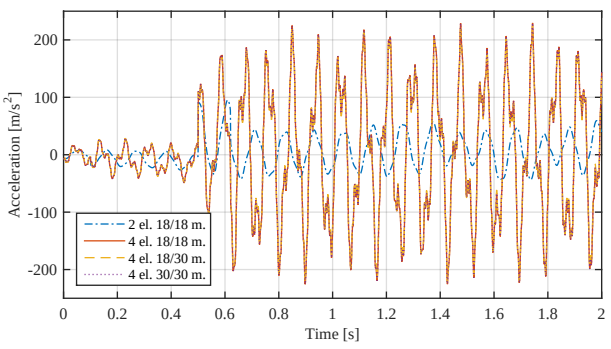

(a) Time domain.

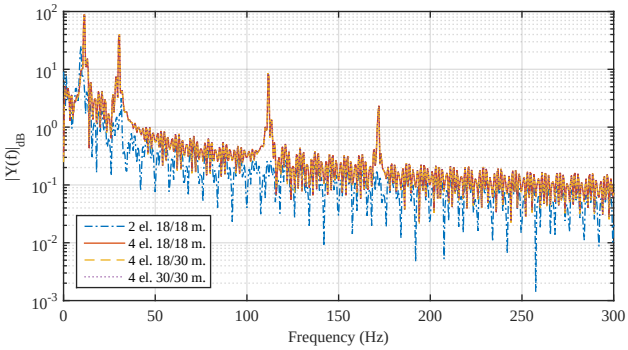

(b) Frequency domain.

Figure 6 Comparison of the tip z-coordinate acceleration of the L-shaped mechanism under torque input.

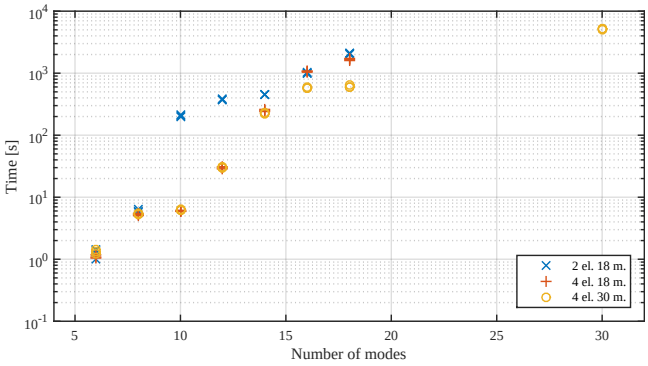

Figure 7 Computational time [s] in logarithmic scale, mechanism subjected to torque input.

As in gravitational force modality, also in this case we can assume that, by means of ERLS-CMS model with a number of modes lower than the maximum one, the reduction of computational effort is of great significance.
It has to be noticed that the results obtained in this paper have been obtained with a model suitable for small displacements and small elastic deformations. By considering longer rods or by increasing the stiffness of the material, a more

flexibility would be introduced and this fact could lead to large elastic deformations. In such a condition, the Equivalent Rigid-Link System formulation could not be adopted any more being the approach not suitable to cope with large elastic deformations.

6 CONCLUSION AND FUTURE WORKS

In this paper, a numerical formulation and comparison between a Finite Element Method and a Component Mode Synthesis approach, based on a Equivalent Rigid-Link System 3-D dynamic formulation, have been presented. The kinematics and dynamics equations have been recalled and a theoretical comparison between the two approaches discussed. Then, the models have been numerically implemented in Matlab^{TM} environment, a L-shape manipulator has been chosen as a benchmark system and different simulations have been run both under gravity and torque inputs by varying, in particular, the number of considered modes.
With respect to the Equivalent Rigid-Link System - Finite Element Method implementation, given the fact that the new formulation allows to reduce the number of DoFs of the considered system, the computational time required decreases. Indeed, it is highly dependent on the number of DoFs, now the number of kept modes and their frequency; however, as demonstrated, the Equivalent Rigid-Link System - Component Mode Synthesis approach allows to keep both the gross and the fine motion of the robotic system. Since the choice of the selected modes could be made in different manners, in future works, different modal reduction strategies will be applied and evaluated for increasing the performance of the developed approach.

REFERENCES

[1] IFToMM, International Federation for the Promotion of Mechanism and Machine Science. `www.iftomm-multibody.org/benchmark/`, 2017. [Online; accessed 29-September-2017].

[2] O. A. Bauchau. *Flexible Multibody Dynamics*. Springer, 2011.

[3] Olivier A Bauchau, Peter Betsch, Alberto Cardona, Johannes Gerstmayr, Ben Jonker, Pierangelo Masarati, and Valentin Sonneville. Validation of flexible multibody dynamics beam formulations using benchmark problems. *Multibody System Dynamics*, 37(1):29–48, 2016.

[4] M. Benosman, F. Boyer, G.L. Vey, and D. Primautt. Flexible links manipulators: from modelling to control. *Journal of Intelligent and Robotic Systems*, 34(4):381–414, August 2002.

[5] P Boscariol, P Gallina, A Gasparetto, M Giovagnoni, L Scalera, and R Vidoni. Evolution of a dynamic model for flexible multibody systems. In *Advances in Italian Mechanism Science*, pages 533–541. Springer, 2017.

[6] H. Bremer. *Elastic Multibody Dynamics*. Springer, 2008.

[7] R. Caracciolo, D. Richiedei, A. Trevisani, and V. Zanotto. Robust mixed-norm position and vibration control of flexible link mechanisms. *Mechatronics*, 15(7):767–791, September 2005.

[8] L.W. Chang and J.F. Hamilton. The kinematics of robotic manipulators with flexible links using an equivalent rigid link system (erls) model. *ASME Journal of Dynamic Systems, Measurement and Control*, 113:48–53, 1991.

[9] R.R. Craig and M.C.C. Bampton. Coupling of substructures for dynamics analyses. *AIAA Journal*, 6(7):1313–1319, 1968.

[10] Alessandro De Luca and Wayne J Book. Robots with flexible elements. In *Springer Handbook of Robotics*, pages 243–282. Springer, 2016.

[11] S. Dietz, O. Wallrapp, and S. Wiedemann. Nodal vs. modal representation in flexible multibody system dynamics. In *Proceeding of Multibody Dynamics 2003, IDMEC/IST 2003*, pages 1–4, Lisbon, Portugal, 2003.

[12] S.K. Dwivedy and P. Eberhard. Dynamic analysis of flexible manipulators, a literature review. *Mechanism and Machine Theory*, 41:749–777, 2006.

[13] D. Garcia-Vallejo, J. Mayo, J.L. Escalona, and J. Dominguez. Three-dimensional formulation of rigid-flexible multibody systems with flexible beam elements. *Multibody Systems Dynamics*, 20:1–28, 2008.

[14] A. Gasparetto. Accurate modelling of a flexible-link planar mechanism by means of a linearized model in the state-space form for design of a vibration controller. *Journal of Sound and Vibration*, 240(2):241–262, 2001.

[15] A. Gasparetto and V. Zanotto. Vibration reduction in a flexible-link mechanism through synthesis of an optimal controller. *Meccanica*, 6(6):611–622, December 2006.

[16] Alessandro Gasparetto, Amir Kiaeian Moosavi, Paolo Boscariol, and Marco Giovagnoni. Experimental validation of a dynamic model for lightweight robots. *Int J Adv Robot Syst*, 10(182), 2013.

[17] S.S. Ge, T.H. Lee, and G. Zhu. Nonlinear feedback controller for a single-link flexible manipulator based on finite element model. *J. Robotic Systems*, 14(3):165–178, 1997.

[18] M. Giovagnoni. A numerical and experimental analysis of a chain of flexible bodies. *ASME Journal of Dynamic Systems, Measurement and Control*, 116:73–80, 1994.

[19] Manuel González, Urbano Lugrís, Ruth Gutiérrez, and Javier Cuadrado. Benchmarking of MBS simulation software. In *ASME 2005 International Design Engineering Technical Conferences and Computers and*

Information in Engineering Conference, pages 1885–1894. American Society of Mechanical Engineers, 2005.

[20] Xin Jiang, Atsushi Konno, and Masaru Uchiyama. Vision-based task-level control of a flexible-link manipulator. *Advanced Robotics*, 24(4):467–488, 2010.

[21] Cheng Liu Qiang Tian Kai Luo, Haiyan Hu. Model order reduction of flexible multibody systems described by the ANCF. In *ECCOMAS Thematic Conference on Multibody Dynamics*, 2017.

[22] P. Kalra and A.M. Sharan. Accurate modeling of flexible manipulators using finite element analysis. *Mechanism and Machine Theory*, 26:299–313, 1991.

[23] Hideaki Kanoh. Distributed parameter models of flexible robot arms. *Advanced robotics*, 5(1):87–99, 1990.

[24] J.M. Martins, Z. Mohamed, M.O. Tokhi, J. Sa da Costa, and M.A. Botto. Approaches for dynamic modelling of flexible manipulator systems. In *Proceedings of the IEEE Conference on Control Theory Appl.*, volume 150, July 2003.

[25] G. Naganathan and A.H. Soni. Nonlinear modeling of kinematic and flexibility effects in manipulator design. *ASME Journal of Mechanisms, Transmission and Automation in Design*, 110:243–254, 1988.

[26] S. Nagarajan and D.A. Turcic. Lagrangian formulation of the equations of motion for elastic mechanisms with mutual dependence between rigid body and elastic motions. part i: element level equations. *ASME Journal of Dynamic Systems, Measurements, and Control*, 112:203–214, 1990.

[27] HN Rahimi and M Nazemizadeh. Dynamic analysis and intelligent control techniques for flexible manipulators: a review. *Advanced Robotics*, 28(2):63–76, 2014.

[28] A.A. Shabana. Flexible multibody dynamics: Review of past and recent developments. *Multibody System Dynamics*, 1:189–222, 1997.

[29] A.A. Shabana. *Dynamics of Multibody systems, 3rd ed*. Cambridge University press, 2005.

[30] R.J. Theodore and A. Ghosal. Comparison of the assumed modes method and finite element models for flexible multilink manipulators. *Int. J. Robotics Res.*, 14(2):91–111, 1995.

[31] M.O. Tokhi and A.K.M. Azad. *Flexible Robot Manipulators: Modeling, Simulation and Control*. Control Engineering Series, The Institution of Engineering and Technology (IET), 2008.

[32] D.A. Turcic and A. Midha. Dynamic analysis of elastic mechanism systems. part i: applications. *ASME Journal of Dynamic Systems, Measurement and Control*, 106:249–254, 1984.

[33] D.A. Turcic and A. Midha. Generalized equations of motion for the dynamic analysis of elastic mechanism systems. *ASME Journal of Dynamic Systems, Measurement and Control*, 106:242–248, 1984.

[34] D.A. Turcic, A. Midha, and J.R. Bosnik. Dynamic analysis of elastic mechanism systems. part ii: experiment results. *ASME Journal of Dynamic Systems, Measurement and Control*, 106:255–260, 1984.

[35] Renato Vidoni, Paolo Gallina, Paolo Boscariol, Alessandro Gasparetto, and Marco Giovagnoni. Modeling the vibration of spatial flexible mechanisms through an Equivalent Rigid-Link System/Component Mode Synthesis approach. *Journal of Vibration and Control,*, 23(12):1890–1907, 2017.

[36] Renato Vidoni, Alessandro Gasparetto, and Marco Giovagnoni. Design and implementation of an erls-based 3-d dynamic formulation for flexible-link robots. *Robot. Comput.-Integr. Manuf.*, 29(2):273–282, 2013.

[37] Renato Vidoni, Alessandro Gasparetto, and Marco Giovagnoni. A method for modeling three-dimensional flexible mechanisms based on an equivalent rigid-link system. *Journal of Vibration and Control*, 20(4):483–500, 2014.

[38] O.A. Wallrapp. Standardization of flexible body modeling in multibody system codes, part i: Definition of standard input data. *Mechanics of Structures and Machines*, 22(3):283–304, 1994.

[39] D.L.W. Wang, Y.F. Lu, Y. Liu, and X.G. Li. Dynamic model and tip trajectory tracking control for a two-link flexible robotic manipulator. In *Proceedings of the IEEE Conference on System, Man and Cybernetics*, pages 1020–1024, Beijing, 1996.

[40] Tamer M Wasfy and Ahmed K Noor. Computational strategies for flexible multibody systems. *Applied Mechanics Reviews*, 56(6):553–613, 2003.

[41] ZW Zhang, YX Wu, JG Liu, W Ren, and MH Cao. Research on the rigid-flexible multibody dynamics of concrete placing boom. *Automation in Construction*, 67:22–30, 2016.